Synthesis and Reactivity of Fe(II) Complexes Containing *cis* Ammonia Ligands

Alexander S. Phearman and R. Morris Bullock*

Center for Molecular Electrocatalysis, Pacific Northwest National Laboratory, Richland, Washington, 99352, United States

KEYWORDS (Ammonia, Electrochemistry, Iron, Organometallics, Crystallography, hydrogen atom abstraction)

ABSTRACT: The development of earth-abundant transition metal complexes for electrocatalytic ammonia oxidation is needed to facilitate a renewable energy economy. Important to this goal is a fundamental understanding of how ammonia binds to complexes as a function of ligand geometry and electronic effects. We report the synthesis and characterization of a series of Fe(II)–NH_3 complexes supported by tetradentate, facially-binding ligands with a combination of pyridine and *N*-heterocyclic carbene donors. Electronic modification of the supporting ligand led to significant shifts in the $Fe^{III/II}$ potential and variations in NH bond acidities. Finally, investigations of ammonia oxidation by cyclic voltammetry, controlled potential bulk electrolysis, and through addition of stoichiometric organic radicals TEMPO and $^{tBu3}ArO^{\bullet}$ are reported. No catalysis of oxidation of NH_3 to N_2 was observed, and $^{15}N_2$ was detected only in reactions with $^{tBu3}ArO^{\bullet}$.

The transition from a fossil fuel-based system to a sustainable economy requires discovery of new scientific principles that support the development of clean technologies. While progress has been made in the design and implementation of renewable, carbon-neutral energy production, further advances are needed in large scale energy storage because of solar and wind energy sources are intermittent. Ammonia has been targeted as a potential carbon-free energy storage solution because of its high energy density and ease of liquefaction.[1] In addition, adoption of ammonia as an energy storage vector would be facilitated because of ammonia's large-scale use as a fertilizer and the existing storage and distribution networks.

While NH_3 can be used as a fuel in internal combustion engines, significant improvement in efficiency and reduction in NO_x emissions can be realized if the six-electron, six proton oxidation of NH_3 to N_2 is carried out electrochemically in a fuel cell (Equation 1). Fundamental studies of NH_3 binding and oxidation by transition metals will facilitate the design of catalytic ammonia oxidation technology.

$$2\,NH_3 \longrightarrow N_2 + 6\,e^- + 6\,H^+ \qquad (1)$$

Ammonia is a classical ligand in coordination chemistry, and its oxidation and coupling mediated by transition metals has been demonstrated. Collman and coworkers found that the formal removal of $H^{\bullet}$ (via oxidation and deprotonation) from cofacial Ru porphyrins resulted in N–N coupling to give a binuclear Ru(μ-N_2H_4)Ru complex.[2] We later reported catalytic NH_3 oxidation to N_2 by [Ru(tetramesitylporphyrin)(NH_3)$_2$] using organic aryloxy compounds as a hydrogen atom abstraction (HAA) reagent.[3] These HAA reagents have also been used for oxidation of M–NH_3 complexes with Cr,[4] Mo,[5] Mn,[6] Os,[7] and Ni[8] complexes, and have the potential to function as mediators that are regenerated at an electrode.[9] Progress has also been made in homogeneous electrochemical ammonia oxidation using Mn,[10] Fe,[11] Cu,[12] and Ru.[13] Llobet and coworkers recently reported an immobilized molecular Ru catalyst that displayed high stability and activity at a potential of 0.1 V vs $Fc^{+/0}$,[14] a significant improvement over the corresponding homogeneous molecular electrocatalyst.[13b]

The key step of N–N bond formation has a large favorable influence on the thermodynamics of oxidation of NH_3.[9a] This step has been proposed to proceed by (a) bimolecular coupling of two M—NH_n species, (b) nucleophilic attack of ammonia on an oxidized M–NH_n species, or (c) coupling of two *cis*-coordinated M(NH_n)(NH_m) species (Figure 1). The coupling of *cis* ligands has only been proposed recently,[11a, b] as most transition metal complexes investigated for

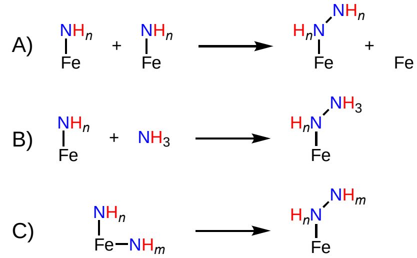

ammonia oxidation have either a single ammonia ligand or two NH_3

Figure 1. Proposed modes of N–N coupling in ammonia oxidation catalysis.

ligands in a *trans*-orientation. Zott and Peters reported an Fe^{II} polypyridyl electrocatalyst for ammonia oxidation that exhibits a turnover number (TON) of 149 equiv. N_2 per Fe.[11b] Their catalyst required an applied potential of +0.85 V vs $Fc^{+/0}$, giving an overpotential of >1.7 V and requiring the use of a boron-doped diamond electrode to avoid deleterious ammonia oxidation at a glassy carbon electrode (onset at ~0.2 V vs $Fc^{+/0}$). In addition, both catalysts proposed to operate by mechanism C were found to be unstable at high [NH_3].

With the goal of addressing the limitations described above and gaining more understanding of the reactivity of transition metal complexes containing *cis*-coordinated ammonia ligands, we sought to identify ligands that would enable retention of the desired binding geometry while allowing the systematic modification of ligand electronics. Kühn and coworkers have developed a series of tetradentate ligands containing both pyridine and *N*-heterocyclic carbene (NHC) donors.[15] When a three carbon linker is installed between the two halves of the ligand, complexes bind these ligands in a facial coordination geometry, binding two *cis* MeCN ligands.

RESULTS AND DISCUSSION

We initially targeted [^{H}(NCCN)Fe($NCCH_3$)$_2$][PF_6]$_2$,[15a] (Scheme 1) where the tetradentate ligand, ^{H}(NCCN), consists of two NHC and two pyridine donors. When [^{H}(NCCN)Fe($NCCH_3$)$_2$]$^{2+}$ is treated with $^{15}NH_3$ (1 atm) a color change from red to dark red was observed upon NH_3 dissolution, giving facile, clean conversion to [^{H}(NCCN)Fe($^{15}NH_3$)$_2$]$^{2+}$ (Scheme 1), which was stable in solution for weeks with <5% decomposition. Two diagnostic doublets for the Fe–$^{15}NH_3$ ligands appeared in the ^{1}H NMR spectrum at 0.19 ($^{1}J_{NH}$ = 67.0 Hz) and 2.48 ppm ($^{1}J_{NH}$ = 65.6 Hz); both collapse to singlets in the ^{1}H{^{15}N} NMR spectra.

Scheme 1. Reaction of Ammonia to Give a *bis*-(NH_3) Complex.

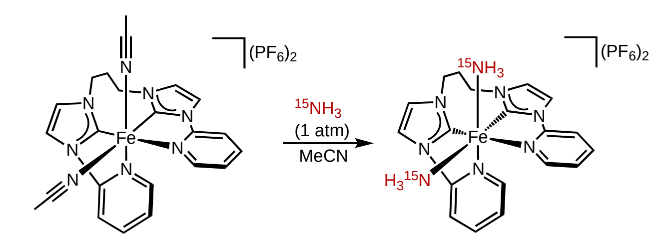

[^{H}(NCCN)Fe($NCCH_3$)$_2$]$^{2+}$ **[^{H}(NCCN)Fe(NH_3)$_2$]$^{2+}$**

The ^{15}N NMR spectrum displays two quartets at −399.4 and −430.4 ppm that are shifted upfield of free $^{15}NH_3$ (−383 ppm), demonstrating a significant difference between pyridine or NHC as *trans* donors. 2D NOESY and selective 1D NOESY NMR experiments allow assignment of the -399.4 ppm ^{15}N signal to the ammonia ligand *trans* to the NHC and the −430.4 ppm signal to the ammonia ligand *trans* to the pyridine (Figure S9). In the ^{13}C{^{1}H} NMR spectrum, two bond ^{15}N–^{13}C ($^{2}J_{NC}$ = 4 Hz) coupling is observed to the carbene carbon resonance at 216.7 ppm.

When [^{H}(NCCN)Fe($NCCH_3$)$_2$]$^{2+}$ is treated with 0.25 atm $^{15}NH_3$, the formation of [^{H}(NCCN)Fe($^{15}NH_3$)$_2$]$^{2+}$, as well as two isomers of [^{H}(NCCN)Fe(NH_3)($NCCH_3$)]$^{2+}$ are observed, where the single NH_3 ligand is bound *trans* to either a pyridine or NHC. Complete conversion to [^{H}(NCCN)Fe($^{15}NH_3$)$_2$]$^{2+}$ is observed under 1 atm NH_3. Single crystals of [^{H}(NCCN)Fe(NH_3)$_2$]$^{2+}$ were grown under an NH_3 atmosphere, and X-ray diffraction studies show Fe–NH_3 bond lengths of 2.084(2) and 2.047(2) Å for the ammonia ligands *trans* to the NHC (N1) and pyridine (N2), respectively (Figure 2).

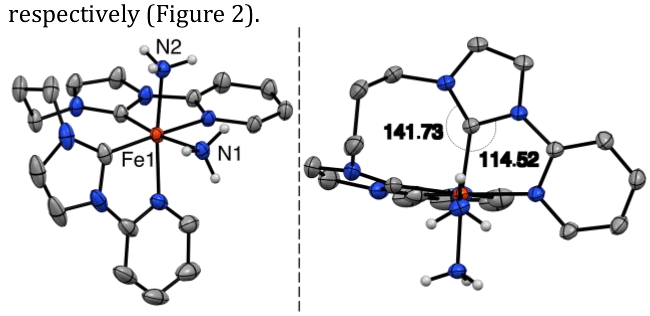

Figure 2. Solid state structure of [^{NMe2}(NCCN)Fe(NH_3)$_2$]$^{2+}$ as determined by X-ray diffraction. Cocrystallized solvent and PF_6 anions are not shown. Thermal ellipsoids are displayed at 50% probability.

These values are consistent with reported values of similar Fe^{II}(NH_3) complexes (2.09 ± 0.07 Å).[11a, b, 16] While adjacent pyridine and NHC's are coplanar, because of the propyl-linker and 5-membered pyridine-NHC chelate, the NHC ligands are slightly twisted, with N_{NHC}-C_{NHC}-Fe angles of 114.5°/141.7° and 115.0°/140.5° away from typical angles of 128° for monodentate NHC transition metal complexes (Figure 2). When these single crystals were redissolved in CD_3CN, a mixture of species was observed due to substitution of NH_3 by CD_3CN.

In electrochemical characterization using cyclic voltammetry, a reversible wave for the $Fe^{III/II}$ couple of [^{H}(NCCN)Fe($NCCH_3$)$_2$]$^{2+}$ occurs at $E_{1/2}$ = +0.55 V vs $Fc^{+/0}$ in MeCN (Figure 3). In the presence of NH_3 (~1.8 M), a significant cathodic shift is observed, with a new, irreversible $Fe^{III/II}$ oxidation with E_{pa} = +0.10 V vs $Fc^{+/0}$ (Figure S48). When the potential was swept to more oxidizing potentials a significant increase in current was observed, but background NH_3 oxidation by the glassy carbon electrode[13e] made it difficult to distinguish possible Fe-mediated ammonia oxidation.[13e, 17] A controlled potential bulk electrolysis experiment at 0.36 V vs $Fc^{+/0}$ with [^{H}(NCCN)Fe($NCCH_3$)$_2$]$^{2+}$ in the presence of NH_3 (1 atm) in MeCN using a carbon felt working electrode only passed 8 e^-/Fe, and no N_2 was detected in the headspace by GC using a thermal conductivity detector.

The reactivity of [^{H}(NCCN)Fe(NH_3)$_2$]$^{2+}$ with organic radicals was also investigated. While of [^{H}(NCCN)Fe(NH_3)$_2$]$^{2+}$ does not react with TEMPO radical under an ammonia atmosphere, it does react with 2,4,6-tri-*tert*-butyl-aryloxy radical (^{t}Bu$_3$ArO•). After 25 h with 13 equiv. ^{t}Bu$_3$ArO• and 0.5 atm $^{15}NH_3$, ^{15}N{^{1}H} NMR spectroscopy revealed formation of a small amount of $^{15}N_2$, as well as larger unidentified peaks at -344.1 and +4.8 ppm (Figure S45). Analysis of the volatiles after vacuum transferring the contents of the sample did not detect any

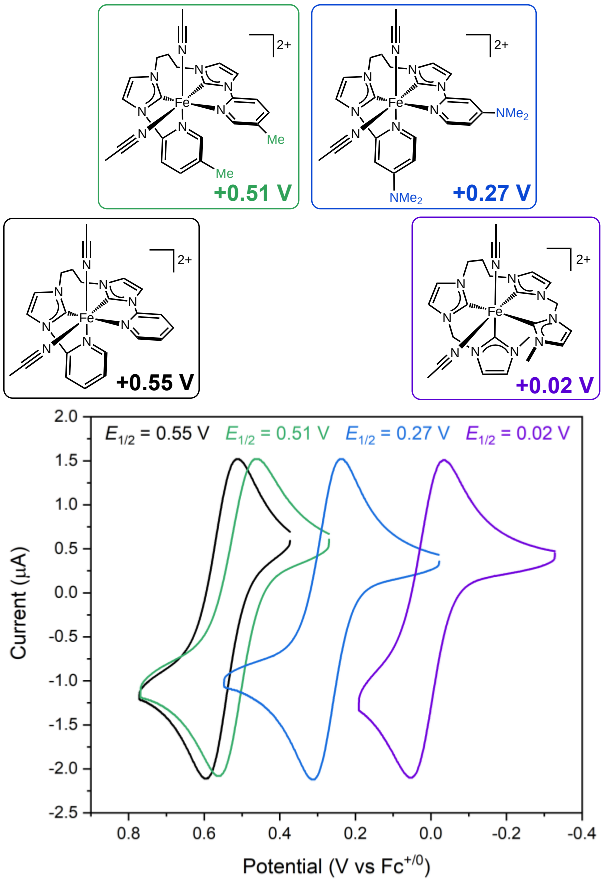

N_2H_4.[18]

Figure 3. Effect of ligand modulation on the $Fe^{III/II}$ couple by cyclic voltametry. $[^{H}(NCCN)Fe(NCCH_3)_2]^{2+}$ (red),[15a] $[^{Me}(NCCN)Fe(NCCH_3)_2]^{2+}$ (green), $[^{NMe2}(NCCN)Fe(NCCH_3)_2]^{2+}$ (blue), and (*tetra*-NHC)$Fe(NCCH_3)_2]^{2+}$ (purple)[19] are shown.

Inspired by the work of Smith and Hamann on molecular catalysts for ammonia oxidation[13e] and others on the electronic effect of NMe_2 substitution,[20] we sought to shift the $Fe^{III/II}$ couple cathodically through substitution of the pyridines of the ligand. A Me-substituted ligand, ^{Me}(NCCN), and a NMe_2-substituted ligand, ^{NMe2}(NCCN), were both synthesized.

Imidazolyl-pyridines were synthesized through reaction of substituted 2-bromopyridines and K_2CO_3 in neat imidazole, and were easily purified by flash column chromatography. Subsequent reaction of the substituted imidazolyl-pyridines (2 equiv.) with 1,3-dibromopropane proceed smoothly in 1,4-dioxane before anion exchange to give the desired ligands ^{Me}(NCCN) (77% yield) and ^{NMe2}(NCCN) (71% yield) as white solids (Scheme 2). The use of 1,4-dioxane as solvent avoided pressurization of reaction vessels and gave comparable yields to similar literature synthesis that utilized THF at 100°C. Metalation of ^{Me}(NCCN) and ^{NMe2}(NCCN) were carried out using $Fe[N(SiMe_3)_2]_2$ to give $[^{R}(NCCN)Fe(NCCH_3)_2][PF_6]_2$ (R = Me (98%) and NMe_2 (79%)).

$[^{Me}(NCCN)Fe(NCCH_3)_2]^{2+}$ reacts with NH_3 in a very similar fashion as the ^{H}(NCCN) analogue, forming $[^{Me}(NCCN)Fe(NH_3)_2]^{2+}$ under 1 atm of NH_3 and a mixture of $[^{Me}(NCCN)Fe(NH_3)_2]^{2+}$ and both isomers of $[^{Me}(NCCN)Fe(NH_3)(NCCH_3)_2]^{2+}$ under 0.25 atm $^{15}NH_3$, as observed by NMR spectroscopy. Four distinct $Fe–^{15}NH_3$ doublets are observed in the ^{1}H NMR spectrum (Figure S24), and four peaks are observed in the $^{15}N\{^{1}H\}$ NMR spectrum (Figures 4, S25). $[^{Me}(NCCN)Fe(NCCH_3)_2]^{2+}$ and $[^{Me}(NCCN)Fe(NH_3)_2]^{2+}$ were also both characterized by single crystal x-ray diffraction (Figures S55, S56).

Scheme 2. Synthesis of ^{Me}(NCCN) and ^{NMe2}(NCCN)

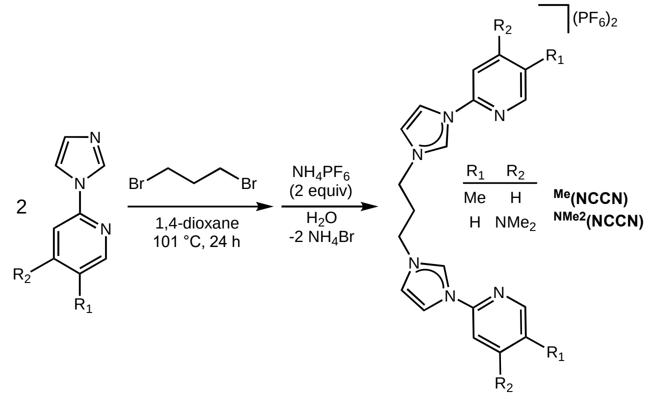

Cyclic voltammetry experiments show that the $Fe^{III/II}$ couple only shifts by 40 mV as a result of the addition of two methyl groups (Figure 3). This small electronic effect is expected to have only a small influence on reactivity in comparison to $[^{H}(NCCN)Fe(NCCH_3)_2]^{2+}$, so CV and bulk electrolysis studies under NH_3 were not pursued.

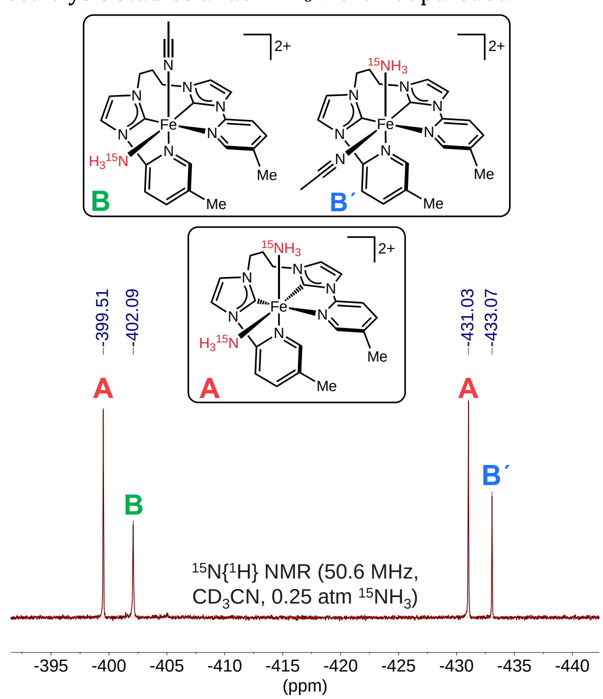

Figure 4. $^{15}N\{^{1}H\}$ NMR spectrum of $[^{Me}(NCCN)Fe(NCCH_3)_2]^{2+}$ under 0.25 atm $^{15}NH_3$. Assignment of peaks is based on NOESY NMR experiments of $[^{H}(NCCN)Fe(NH_3)_2]^{2+}$.

The more electron-donating ligand in $[^{NMe2}(NCCN)Fe(NCCH_3)_2]^{2+}$ results in a –280 mV shift (to +0.27 V vs $Fc^{+/0}$) in the $Fe^{III/II}$ couple, relative to $[^{H}(NCCN)Fe(NCCH_3)_2]^{2+}$ (Figure 3). When a degassed solution of $[^{NMe2}(NCCN)Fe(NCCH_3)_2]^{2+}$ was exposed to $^{15}NH_3$ (0.25 atm), four new signals are observed in the $^{15}N\{^{1}H\}$

NMR spectrum, as well as four Fe–$^{15}NH_3$ signals in the ^1H NMR spectrum, again consistent with

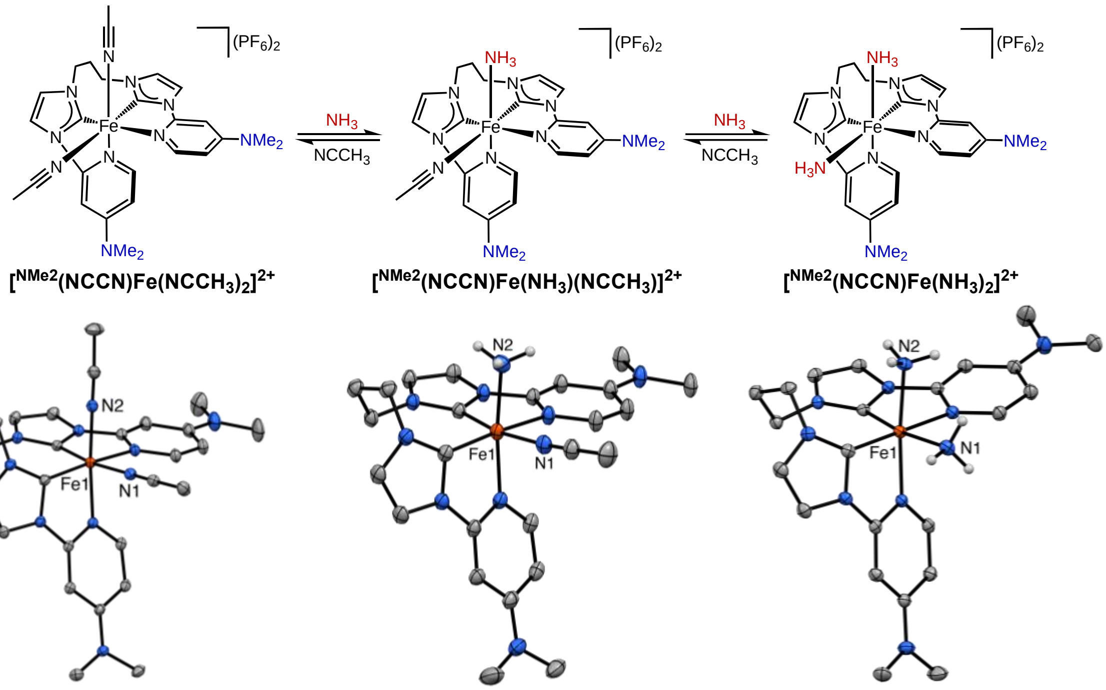

Figure 5. Equilibrium between $[^{NMe2}(NCCN)Fe^{II}(NCCH_3)_2]^{2+}$, $[^{NMe2}(NCCN)Fe^{II}(NH_3)(NCCH_3)]^{2+}$, and $[^{NMe2}(NCCN)Fe^{II}(NH_3)_2]^{2+}$, and structures from single crystal X-ray diffraction studies. Cocrystallized solvent and PF_6 anions are not shown. Thermal ellipsoids are displayed at 50% probability.

formation of both isomers of $[^{NMe2}(NCCN)Fe(NH_3)(NCCH_3)]^{2+}$. Under 1 atm $^{15}NH_3$, $[^{NMe2}(NCCN)Fe(^{15}NH_3)_2]^{2+}$ was the sole product observed. $^{15}N\{^1H\}$ NMR spectroscopy shows that NMe_2-substitution of the pyridine results in a 1.4 ppm upfield shift in the signal for N2 and a 0.4 ppm downfield shift in the signal for N1, comparing $[^{H}(NCCN)Fe(^{15}NH_3)_2]^{2+}$ and $[^{NMe2}(NCCN)Fe(^{15}NH_3)_2]^{2+}$. Comparison of the ^1H NMR spectra of the same two compounds shows upfield shifts of the protons on both the N1 (Δ = -0.09 ppm) and N2 (Δ = -0.34 ppm) ammonia signals in $[^{NMe2}(NCCN)Fe(^{15}NH_3)_2]^{2+}$. Thus, larger changes are observed in the Fe–NH_3 *trans* to the pyridine, as expected.

Through vapor diffusion of Et_2O into concentrated MeCN solutions of $[^{NMe2}(NCCN)Fe(NCCH_3)_2]^{2+}$ with varying concentrations of NH_3, single crystals of $[^{NMe2}(NCCN)Fe(NCCH_3)_2]^{2+}$ (no NH_3 present), $[^{NMe2}(NCCN)Fe(NH_3)(NCCH_3)]^{2+}$, and $[^{NMe2}(NCCN)Fe(NH_3)_2]^{2+}$ were obtained and analyzed by X-ray crystallography (Figure 5). The same crystallization conditions used to characterize $[^{H}(NCCN)Fe(NH_3)_2]^{2+}$ resulted in $[^{NMe2}(NCCN)Fe(NH_3)(NCCH_3)]^{2+}$, suggesting that the more electron-rich ^{NMe2}(NCCN) ligand leads to lower affinity for ammonia. Minor elongations of the Fe–N2 bond is observed moving from $[^{NMe2}(NCCN)Fe(NCCH_3)(NH_3)]^{2+}$ to $[^{NMe2}(NCCN)Fe(NH_3)_2]^{2+}$, from 2.0363(17) Å to 2.0513(12) Å, but the overall structural parameters do not change significantly between the three structures with the ^{NMe2}(NCCN) ligand.

When $[^{NMe2}(NCCN)Fe(NCCH_3)_2]^{2+}$ is dissolved in MeCN that is saturated with NH_3, a 460 mV cathodic shift in the $Fe^{III/II}$ couple is observed to -0.19 V vs $Fc^{+/0}$ (Figure 6). In contrast to $[^{H}(NCCN)Fe(NCCH_3)_2]^{2+}$, the $Fe^{III/II}$ couple is reversible under NH_3 (Figure 7). When CV data are collected under lower $[NH_3]$ (0.5 M), an additional oxidation feature attributed to $[^{NMe2}(NCCN)Fe(NH_3)(NCCH_3)]^{2+}$ is observed

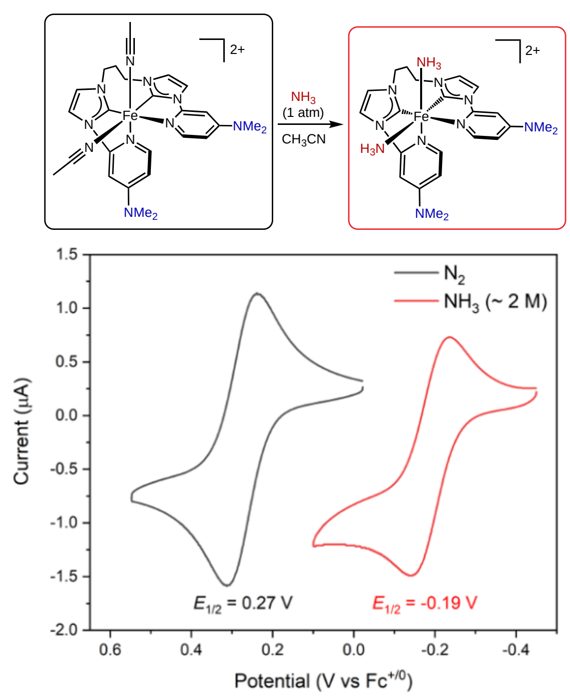

approximately halfway between $[^{NMe2}(NCCN)Fe(NH_3)_2]^{2+}$

Figure 6. Cyclic voltammograms of 1 mM $[^{NMe2}(NCCN)Fe^{II}(NCCH_3)_2]^{2+}$ (red, under N_2) and

$[^{NMe2}(NCCN)Fe^{II}(NH_3)_2]^{2+}$ (blue, ~2 M NH_3) in MeCN with 100 mM [nBu$_4$][PF_6].

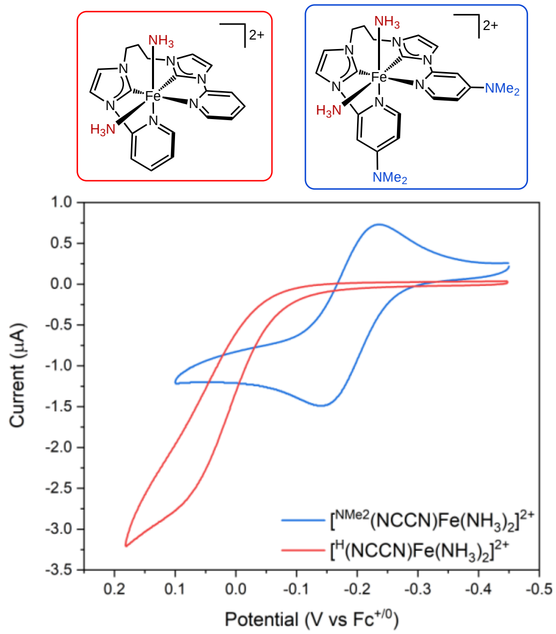

Figure 7. Cyclic voltamagrams of $[^{H}(NCCN)Fe(NH_3)_2]^{2+}$ (red) and $[^{NMe2}(NCCN)Fe(NH_3)_2]^{2+}$ (blue) in MeCN with ~2 M NH_3 with 100 mM [nBu$_4$][PF_6].

and $[^{NMe2}(NCCN)Fe(NCCH_3)_2]^{2+}$ (E_{pa} = 0.05 V vs Fc$^{+/0}$). Scan rate dependency studies indicate that equilibration of $Fe^{II}(NH_3)_2$, $Fe^{II}(NH_3)(NCCH_3)$, and $Fe^{II}(NCCH_3)_2$ is occurring on the CV time scale (Figure S49 - 50). At fast scan rates (up to 10 V/s), the oxidation feature for the $Fe^{II}(NH_3)_2$ at -0.19 V passes less current, and the waves corresponding to the $Fe^{II}(NH_3)(NCCH_3)$ and $Fe^{II}(NCCH_3)_2$, at 0.05 V and +0.27 V, respectively, increase in current. At scan rates down to 25 mV/s, the wave at -0.19 V is much larger, indicating that as the $Fe^{II}(NH_3)_2$ is oxidized at the electrode, the equilibria of $Fe^{II}(NH_3)_2$, $Fe^{II}(NH_3)(NCCH_3)$, and $Fe^{II}(NCCH_3)_2$ replenishes the concentration of $[^{NMe2}(NCCN)Fe^{II}(NH_3)_2]^{2+}$ near the electrode, resulting in a larger proportional current passed.

The irreversible electrochemical behavior of $[^{H}(NCCN)Fe^{II}(NH_3)_2]^{2+}$ under an NH_3 atmosphere is potentially caused by deprotonation of $[^{H}(NCCN)Fe^{III}(NH_3)_2]^{3+}$ by free NH_3 (pK_a = 16.46 in MeCN for NH_4^+),[21] and similar reactions are proposed in mechanisms of electrocatalytic ammonia oxidation using NH_3 as the base.[11a, b, 12b]

The deprotonation of the more electron-rich $[^{NMe2}(NCCN)Fe(^{15}NH_3)_2]^{2+}$ after oxidation was then investigated using a base stronger than NH_3. Upon addition of 1,1,3,3-tetramethylguanidine (TMG, pK_a = 23.35 in MeCN for TMG(H)$^+$)[22], reversibility of the $Fe^{III/II}$ is lost and a cathodic shift of the E_{pa} is observed, consistent with deprotonation of the $[^{NMe2}(NCCN)Fe^{III}(NH_3)_2]^{3+}$ that is produced from oxidation at the electrode (Figure 8).[23]

The reactivity of $[^{NMe2}(NCCN)Fe(NH_3)_2]^{2+}$ with organic radicals was also investigated, and similar to the ^{H}(NCCN) analogue, no reaction was observed between $[^{NMe2}(NCCN)Fe(NCCH_3)_2]^{2+}$ and TEMPO in the absence or presence of NH_3 by ^{1}H NMR spectroscopy. In the absence of NH_3, no reaction was observed between

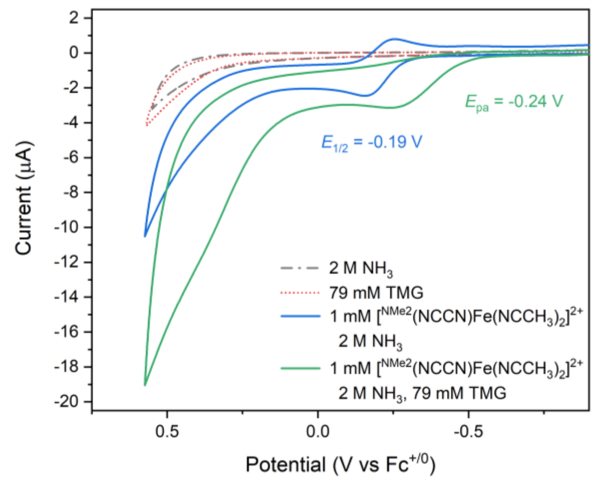

Figure 8. Cyclic voltammograms of 1 mM $[^{NMe2}(NCCN)Fe(NH_3)_2]^{2+}$ and 2M NH_3 in the absence (blue) and presence (green) of 79 mM TMG with 100 mM [nBu$_4$][PF_6] in MeCN. Background oxidation of NH_3 (gray dashes) and TMG (red dots) are also shown.

$[^{NMe2}(NCCN)Fe(NCCH_3)_2]^{2+}$ (13 mM) and ^{t}Bu$_3$ArO$^\bullet$ (11 equiv.) either. When $^{15}NH_3$ (1 atm) was added, the dark blue color of ^{t}Bu$_3$ArO$^\bullet$ faded over 30 min, and ^{t}Bu$_3$ArOH was observed by ^{1}H NMR spectroscopy. An overnight ^{15}N NMR experiment showed formation of $^{15}N_2$ and an unidentified species at -254.5 ppm. Analysis of the headspace of the NMR tube by GC-TCD showed 1 equiv. N_2 formation. A similar reaction with $[^{NMe2}(NCCN)Fe(NCCH_3)_2]^{2+}$ (4.7 mM), $^{15}NH_3$ (1 atm), and higher [^{t}Bu$_3$ArO$^\bullet$] (288 mM, 61 equiv.) gives similar results as with the ^{H}(NCCN) analogue, with a small amount of $^{15}N_2$ observed as well as unidentified resonances at -345.1 and +4.0 ppm.

Kühn and coworkers reported an $Fe^{II}(NCCH_3)_2$ complex with a facially-binding tetradentate NHC ligand ([(*tetra*-NHC)Fe(NCCH$_3$)$_2$][PF$_6$]$_2$)[19] (Figure 9) and have demonstrated nicely that replacing pyridine donors with NHC ligands systematically shifts the $Fe^{III/II}$ couple when ligated to Fe.[15b] While the binding geometry is very similar to the ^{R}(NCCN) complexes discussed above, the $Fe^{III/II}$ couple is shifted even further cathodically to +0.02 V vs $Cp_2Fe^{+/0+}$ (Figure 2).

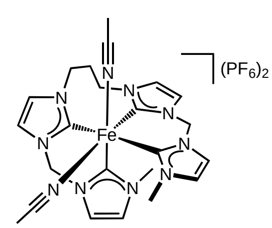

[(*tetra*-NHC)Fe(NCCH$_3$)$_2$][PF$_6$]$_2$

Figure 9. **[**(*tetra*-NHC)Fe(NCCH$_3$)$_2$][PF$_6$]$_2$ reported by Kühn and coworkers.[19]

When a CD_3CN solution of [(*tetra*-NHC)Fe(NCCH$_3$)$_2$]$^{2+}$ was placed under $^{15}NH_3$ (1 atm) in an NMR tube, partial conversion to a new species was observed. Only one Fe–$^{15}NH_3$ peak is observed, at 1.48 ppm ($^1J_{NH}$ = 66.4 Hz). Due to abundance of NMR signals arising from many diastereotopic hydrogens and low symmetry (*C₁*) of these complexes, accurate NMR integration was hampered, but conversion of $[(\textit{tetra}\text{-NHC})Fe(NCCH_3)_2]^{2+}$ was estimated as 40%.

A $^{15}N\{^1H\}$ NMR experiment showed a single ^{15}N signal at -415.7 ppm, compared to -398.6 and -433.7 ppm signals for $[^{NMe2}(NCCN)Fe(NH_3)_2]^{2+}$. The *mono*-$NH_3$ isomers for $[^{NMe2}(NCCN)Fe(NH_3)(NCCH_3)]^{2+}$ give ^{15}N signals at -401.0 ppm ($^{15}NH_3$ *trans* to the NHC donor) and -433.3 ppm ($^{15}NH_3$ *trans* to the NMe_2-pyridine donor).

While $[(\textit{tetra}\text{-NHC})Fe(NCCH_3)_2]^{2+}$ has four NHC donors, the two labile binding sites are distinct, as one has steric pressure from a wingtip NHC methyl group. When Kühn and coworkers added PMe_3 (4 equiv) to $[(\textit{tetra}\text{-NHC})Fe(NCCH_3)_2]^{2+}$ only a single substitution was observed, forming $[(\textit{tetra}\text{-NHC})Fe(PMe_3)(NCCH_3)]^{2+}$.[19] Furthermore, only a single isomer of $[(\textit{tetra}\text{-NHC})Fe(PMe_3)(NCCH_3)]^{2+}$ was observed in solution and in the structure determined by crystallography.

The appearance of a single Fe–$^{15}NH_3$ resonance by ^1H and ^{15}N NMR spectroscopy and CV data are consistent with formation of $[(\textit{tetra}\text{-NHC})Fe(^{15}NH_3)(NCCH_3)]^{2+}$. Our data currently cannot distinguish if only a single isomer is present due to steric constraints or if the two isomers are in rapid exchange on the NMR time scale, leading to signal averaging.

Cyclic voltammetry studies of $[(\textit{tetra}\text{-NHC})Fe(NCCH_3)_2]^{2+}$ in NH_3-saturated MeCN (~2 M) show the formation of several new quasi-reversible redox events at -0.66 V (ΔE_p= 69 mV) and -0.29 V (ΔE_p= 151 mV) with a scan rate of 100 mV/s (Figure 10). Given the similarities to CV data of $[^{NMe2}(NCCN)Fe(NCCH_3)_2]^{2+}$ in the presence of lower $[NH_3]$, the redox feature at -0.29 V is attributed to $[(\textit{tetra}\text{-NHC})Fe(NH_3)(NCCH_3)]^{2+}$ and the smaller couple at -0.66 V is attributed to of $[(\textit{tetra}\text{-NHC})Fe(NH_3)_2]^{2+}$. This would constitute a 310 mV shift for the first substitution of bound MeCN for NH_3 and a 370 mV shift for the second substitution.

While ΔE_p = 69 mV for the $Fe^{III/II}(NH_3)_2$ is close to the idealized 59 mV, ΔE_p mV for $Fe^{III/II}(NH_3)(NCCH_3)$ is much larger (151 mV). The ratio of cathodic and anodic peak currents, i_{pc}/i_{pa}, is 1.05 for the couple at the $Fe^{III/II}(NH_3)_2$ and 0.92 for the $Fe^{III/II}(NH_3)(NCCH_3)$ at 100 mV/s. The data are consistent with an equilibrium between the $Fe(NH_3)_n(NCCH_3)_m$ ($n + m = 2$) species on the CV time scale. When the scan rate is increased to 2000 mV/s, the $Fe^{III/II}(NCCH_3)_2$ is also observed ($E_{1/2}$= +0.02 V) and the current passed for the two earlier oxidation waves decreases when normalized for scan rate.

CONCLUSIONS

A series of $Fe^{II}(NH_3)_2$ and $Fe^{II}(NH_3)(NCCH_3)$ complexes with facially-coordinating, tetradendate ligands have been synthesized and characterized to better understand ammonia binding and activation. This report demonstrates the balance of supporting ligand binding strength, stability, and electron density on the metal with the ability to bind multiple NH_3 ligands to one metal center. From $[^{H}(NCCN)Fe(NH_3)_2]^{2+}$ to $[(\textit{tetra}\text{-NHC})Fe(NH_3)_2]^{2+}$, a 600 mV range was observed in the $Fe^{III/II}$ couple. Over this range, a significant change in the ability to bind two NH_3 ligands was observed, with the very electron-rich (*tetra*-NHC) ligand resulting in primarily monosubstituted $Fe(NH_3)(NCCH_3)$ complexes even under high $[NH_3]$. A significant difference in the pK_a of the oxidized $[^{R}(NCCN)Fe^{III}(NH_3)_2]^{3+}$ complexes was also observed. With the ^{H}NCCN ligand, results were consistent with deprotonation of the Fe^{III}–NH_3 being deprotonated by NH_3 in solution, while the more electron rich ^{NMe2}(NCCN) ligand requires a stronger base the achieve the same result. This has implications in designing electrocatalysts for ammonia oxidation, as careful choice of the base is needed to minimize overpotential while retaining desired reactivity.

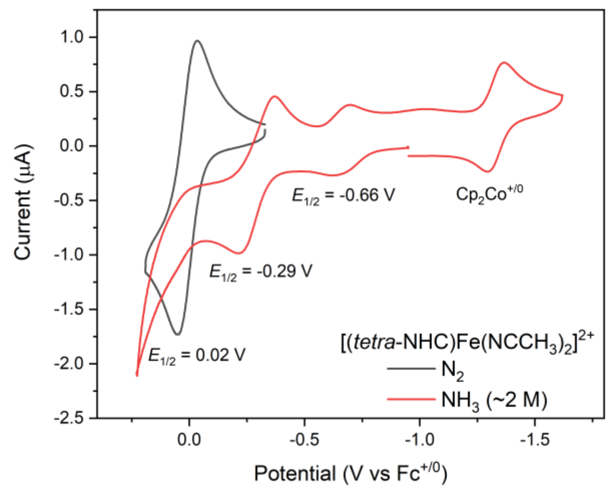

Figure 10. Cyclic voltamagrams of $[(\textit{tetra}\text{-NHC})Fe(NCCH_3)_2]^{2+}$ in MeCN under N_2 (purple) or in an NH_3-saturated solution (red) with 100 mM $[n\text{Bu}_4][PF_6]$ and a scan rate of 100 mV/s. Cp_2CoPF_6 (-1.33 V) is present for internal referencing.

EXPERIMENTAL SECTION

General Considerations. All manipulations were carried out using a nitrogen Schlenk line or a Vacuum Atmospheres nitrogen-filled glovebox unless otherwise specified. Experiments where headspace was sampled to look for N_2 formation by GC-TCD were performed in an argon glovebox. All glassware was dried overnight at 160 °C before use. CD_3CN and $CDCl_3$ was dried over CaH_2, vacuum distilled, and stored over activated 3 Å molecular sieves. NMR spectra were recorded on a Bruker NEO 600 MHz spectrometer equipped with TCI cryoprobe or Bruker NEO 500 MHz spectrometers with SmartProbes. NMR spectra were referenced to the residual solvent peak (^1H, ^{13}C) with $SiMe_4$ defined as 0 ppm.[24] ^{31}P and ^{15}N NMR spectra were referenced to external standards of 85% H_3PO_4 (^{31}P) or $CH_3{}^{15}NO_2$ (^{15}N), both defined as 0 ppm. NMR spectra were recorded at 298 K unless otherwise specified. FT-IR spectra were recorded using a Thermo Scientific NICOLET iS10 spectrometer with a diamond ATR attachment. Elemental analyses were performed by Atlantic Microlab (Norcross, GA).

Acetonitrile, methylene chloride, diethyl ether, pentane, and toluene were dried by passage through columns containing activated alumina and molecular sieves (Innovative Technology, Inc., PureSolv™ solvent purification system). 1,4-dioxane (anhydrous, unstabilized) was purchased from Sigma Aldrich and used as received. Ethyl acetate, chloroform, and methanol used for ligand synthesis used without purification or drying.

5-methyl-2-bromopyridine (98%, TCI), 4-dimethylamino-2-bromopyridine (95%, Ambeed), 1,3-dibromopropane (98%, TCI), imidazole (99%, Aldrich), and TEMPO (98%, Sigma Aldrich) and stored under N_2. $^{15}NH_3$ (98% purity) was purchased from Cambridge Isotope Laboratories, Inc and NH_3 was purchased from Matheson.

$[^{H}(NCCN)Fe(NCCH_3)_2][PF_6]_2$ [15a], 2-(1*H*-imidazol-1-yl)-5-methylpyridine[25], and tri-*tert*-butyl phenoxyl radical[26] were synthesized according to the previously reported procedure. 2-(1*H*-imidazol-1-yl)-*N*,*N*-dimethylpyridin-4-amine has previously been reported by a different route.[27]

$[^{H}(NCCN)Fe(NH_3)_2][PF_6]_2$

$[^{H}(NCCN)Fe(NH_3)_2]^{2+}$ was synthesized by exposure of $[^{H}(NCCN)Fe(NCCH_3)_2]^{2+}$ to NH_3 (1 atm) in CD_3CN. Upon dissolution of the NH_3 in solution a rapid color change is observed and NMR analysis shows full conversion to $[^{H}(NCCN)Fe(NH_3)_2]^{2+}$. Single crystals suitable for X-ray diffraction were grown by vapor diffusion of Et_2O into a concentrated MeCN solution of $[^{H}(NCCN)Fe(NH_3)_2]^{2+}$ at 23 °C in a glovebox. The MeCN used for crystallization had been previously sparged with NH_3 (natural abundance). For elemental analysis, single crystals of $[^{H}(NCCN)Fe(NH_3)_2]^{2+}$ were removed from the mother liquor, dried briefly under vacuum. Elemental analysis is satisfactory for the contents of the unit cell determined by single crystal X-ray diffraction studies on the same batch of crystals. $^{15}NH_3$ was used For NMR characterization.

^{1}H NMR (400 MHz, CD_3CN) δ 8.92 (d, *J* = 5.7 Hz, 1H), 8.31 (t, *J* = 7.9 Hz, 1H), 8.20 (d, *J* = 2.3 Hz, 2H), 8.06 (d, *J* = 8.4 Hz, 1H), 7.73 (m, 2H), 7.63 (d, *J* = 8.2 Hz, 1H), 7.51 (d, *J* = 2.3 Hz, 1H), 7.28 (d, *J* = 2.3 Hz, 1H), 6.97 (d, *J* = 5.8 Hz, 1H), 6.78 (t, *J* = 6.6 Hz, 1H), 4.50 – 4.40 (m, 1H), 3.99 (dt, *J* = 15.3, 3.4 Hz, 1H), 3.72 – 3.63 (m, 1H), 2.49 (m, 2H), 2.48 (d, $^1J_{NH}$ = 65.6 Hz, 3H), 2.21 (dd, *J* = 10.7, 5.3 Hz, 2H), 0.19 (d, $^1J_{NH}$ = 67.0 Hz, 3H).

^{13}C{^{1}H} NMR (151 MHz, CD_3CN) δ 219.7, 216.7 (d, *J* = 4 Hz), 156.3 (d, *J* = 8 Hz), 154.3, 152.9, 141.0, 139.0, 129.1, 126.6, 123.5, 121.0, 120.9, 118.9, 112.5, 111.9, 46.9, 46.4, 30.9.

^{15}N{^{1}H} NMR (50.7 MHz, CD_3CN) δ -399.4 (N1), -430.4 (N2).

^{15}N NMR (60.9 MHz, CD_3CN) δ -399.9 (q, $^1J_{NH}$ = 65.7 Hz), -430.0 (q, $^1J_{NH}$ = 66.9 Hz)

Anal. Calcd for $C_{19}H_{24}F_{12}FeN_8P_2$ • (MeCN) • $(Et_2O)_{0.5}$: C, 35.04; H, 4.09; N, 15.99. Found: C, 35.38; H, 4.01; N, 16.58. Single crystals of $[^{H}(NCCN)Fe(NH_3)_2][PF_6]_2$ • (MeCN) • $(Et_2O)_{0.5}$ from the same batch used for XRD analysis were briefly dried under vacuum and sent for elemental analysis.

2-(1*H*-imidazol-1-yl)-*N*,*N*-dimethylpyridin-4-amine

2-(1*H*-imidazol-1-yl)-*N*,*N*-dimethylpyridin-4-amine was synthesized by a modification of a literature procedure.[25] In air, a pear-shaped Schlenk flask was charged with 4-dimethylamino-2-bromopyridine (2.075 g ,10.3 mmol), imidazole (2.28 g, 33.4 mmol, 3.2 equiv.), anhydrous K_2CO_3 (2.99 g, 21.6 mmol, 2.1 equiv.), and a PTFE-coated stir bar. The flask was fitted with a reflux condenser and put under an N_2 atmosphere. The reaction was heated to 180 °C for 24 h, during which the sublimed imidazole was occasionally scraped back into the reaction melt. After cooling to room temperature, H_2O (30 mL) and $CHCl_3$ (20 mL) were added to dissolve the contents of the flask before it was transferred to a separatory funnel. The aqueous layer was extracted with $CHCl_3$ (3 × 100 mL). The combined chloroform fractions were washed with an aqueous K_2CO_3 solution (3 × 60 mL) before removing the solvent under vacuum. The crude product was purified using flash column chromatography (silica gel, 2 × 30 cm column, 100:1 EtOAc:MeOH, R_f = 0.3)[27] to give the product as a white powder (1.26 g, 65% yield).

^{1}H NMR (500 MHz, $CDCl_3$) δ 8.76 (s, 1H), 8.09 (d, *J* = 6.0 Hz, 1H), 7.70 (s, 1H), 7.24 (d, *J* = 1.3 Hz, 1H), 6.63 (d, *J* = 2.3 Hz, 1H), 6.49 (dd, *J* = 6.0, 2.3 Hz, 1H), 3.10 (s, 6H).

$[^{Me}(NCCN)][PF_6]_2$

In a N_2-filled glovebox, a 100 mL Schlenk flask was charged with 2-(1*H*-imidazol-1-yl)-5-methylpyridine (2.993 g, 18.80 mmol), 1,4-dioxane (50 mL), and a PTFE-coated stir bar. Using a Schlenk line, a reflux condenser was fitted to the Schlenk flask and 1,3-dibromopropane (950 µL, 9.36 mmol, 0.5 equiv.) was added by syringe. The solution was refluxed for 65 h before cooling to room temperature to give a colorless solution and white precipitate. In air, the white solid was collected on a glass frit and washed with toluene (20 mL). The solid was then dissolved in H_2O (50 mL) and slowly added to a stirring solution of NH_4PF_6 (3.168 g, 19.44 mmol, 2.1 equiv.) in H_2O (100 mL) to give a flocculant pale yellow solid. The mixture was stirred for 15 minutes before the solid was collected on a glass frit and rinsed with H_2O (2 × 50 mL) to remove excess NH_4PF_6 and NH_4Br, then 20 mL CH_2Cl_2. The product was collected and dried under high vacuum overnight (4.67 g, 77% yield).

^{1}H NMR (600 MHz, CD_3CN) δ 9.28 (t, *J* = 1.7 Hz, 2H), 8.43 – 8.40 (m, 2H), 8.08 (t, *J* = 1.9 Hz, 2H), 7.95 – 7.90 (m, 2H), 7.63 (d, *J* = 8.3 Hz, 2H), 7.61 (t, *J* = 1.9 Hz, 2H), 4.37 (t, *J* = 7.3 Hz, 4H), 2.56 (quintet, *J* = 7.3 Hz, 2H), 2.43 (s, 6H).

^{13}C{^{1}H} NMR (125 MHz, CD_3CN) δ 150.6, 145.3, 141.6, 137.1, 135.0, 124.4, 120.7, 114.5, 47.9, 30.5, 18.0.

Anal. Calcd for $C_{21}H_{24}F_{12}N_6P_2$: C, 38.78; H, 3.72; N, 12.92. Found: C, 38.90; H, 3.70; N, 12.67.

$[^{NMe2}(NCCN)][PF_6]_2$

In a N_2-filled glovebox, a 50 mL Schlenk flask was charged with 2-(1*H*-imidazol-1-yl)-*N*,*N*-dimethylpyridin-4-amine (1.26 g, 6.69 mmol), 1,4-dioxane (35 mL), and a PTFE-coated stir bar. Using a Schlenk line, a reflux condenser was fitted to the Schlenk flask and 1,3-dibromopropane (340 µL, 3.35 mmol, 0.5 equiv.) was added by syringe. The reaction was refluxed for 23 h before cooling to room temperature to give a colorless solution and white precipitate. In air, the white solid was collected on a glass frit and washed with hexanes (80 mL). The solid was then dissolved in H_2O (30 mL) and slowly added to a stirring solution of NH_4PF_6 (1.326 g, 8.13 mmol, 1.2 equiv.) in H_2O (100 mL) to give a flocculant white solid. The mixture was allowed to stir for 5 minutes before the solid was collected on a glass frit and rinsed with H_2O (2 × 50 mL) to remove excess NH_4PF_6 and NH_4Br. The product was collected and dried under high vacuum overnight (1.686 g, 71% yield). Single crystals suitable for X-ray diffraction were grown by slow evaporation of an acetone solution of the product.

^{1}H NMR (600 MHz, CD_3CN) δ 9.28 (t, *J* = 1.8 Hz, 2H), 8.11 (t, *J* = 1.9 Hz, 2H), 8.07 (d, *J* = 6.1 Hz, 2H), 7.59 (t, *J* = 1.9 Hz, 2H), 6.77 (d, *J* = 2.3 Hz, 2H), 6.71 (dd, *J* = 6.1, 2.3 Hz, 2H), 4.37 (t, *J* = 7.2 Hz, 4H), 3.09 (s, 12H), 2.58 (p, *J* = 7.3 Hz, 2H).

^{13}C{^{1}H} NMR (151 MHz, CD_3CN) δ 157.79, 149.60, 148.47, 135.07, 124.06, 120.71, 108.78, 96.28, 47.92, 39.89, 30.49.

Anal. Calcd for $C_{23}H_{30}F_{12}N_8P_2$: C, 38.99; H, 4.27; N, 15.82. Found: C, 39.03; H, 4.22; N, 15.60.

$[^{Me}(NCCN)Fe(NCCH_3)_2][PF_6]_2$

In a nitrogen-filled glovebox, ^{Me}(NCCN) (224 mg, 0.344 mmol) was dissolved in MeCN (6 mL) and placed in a -30 °C freezer for 3 h. The solution of Me(NCCN) was then added to a stirring suspension of $Fe(N(SiMe_3)_2)_2$ • $(THF)_{0.75}$ (151 mg, 0.351 mmol) in cold MeCN (14 mL, -30 °C). The mixture was stirred at ambient temperature for 18 h before being filtered through a 0.2 µm PTFE syringe filter and reduced in volume to 2 mL under vacuum. The dark red solution was extracted with pentane (3 × 7 mL) to remove hexamethyldisilazane ($HN(SiMe_3)_2$, HMDS) formed during the reaction. $[^{NMe2}(NCCN)Fe(NCCH_3)_2][PF_6]_2$ was isolated as a dark red crystalline solid by vapor diffusion of Et_2O and pentane (2:1) into a concentrated MeCN solution at ambient temperature. The crystals were crushed and dried under vacuum. Yield: 268 mg, 98%.

^{1}H NMR (500 MHz, CD_3CN) δ 9.09 (s, 1H), 8.21 – 8.17 (m, 1H), 8.16 (dd, *J* = 14.2, 2.3 Hz, 2H), 7.98 (d, *J* = 8.5 Hz, 1H), 7.66 (d, *J* = 8.3

Hz, 1H), 7.57 (d, J = 8.4 Hz, 1H), 7.54 (d, J = 2.3 Hz, 1H), 7.28 (d, J = 2.2 Hz, 1H), 6.77 (s, 1H), 4.52 – 4.46 (m, 1H), 4.45 – 4.34 (m, 1H), 4.01 (dt, J = 15.4, 3.4 Hz, 1H), 2.63 (s, 3H), 2.50 – 2.40 (m, 1H), 2.32 – 2.20 (m, 2H), 2.02 (s, 3H), 1.96 (s, 6H).

$^{13}C\{^1H\}$ NMR (151 MHz, CD_3CN) δ 213.2, 205.8, 153.9, 153.34, 153.31, 142.4, 141.1, 134.9, 132.1, 129.2, 126.6, 121.4, 119.1, 112.4, 111.7, 46.9z, 46.6, 31.5, 18.4 (CH_3), 17.7 (CH_3).

[^{Me}(NCCN)Fe(NH_3)($NCCH_3$)][PF_6]$_2$

An NMR tube fitted with a PTFE valve was charged with [^{Me}(NCCN)Fe($NCCH_3$)$_2$]$^{2+}$ and CD_3CN in a nitrogen-filled glovebox. The sample was degassed by three freeze-pump-thaw cycles, then pressurized with $^{15}NH_3$ (0.25 atm). The sample was shaken to dissolve the $^{15}NH_3$, and the headspace pressure was replenished several times until the pressure change upon opening the sample was minimal. N_2 was then used to bring the sample to 1 atm total. By ^1H, $^1H\{^{15}N\}$, and $^{15}N\{^1H\}$ NMR spectroscopy, a mixture of $Fe(NH_3)_n(NCCH_3)_m$ species, were observed ($n + m = 2$). NMR data reported below are for signals readily assigned to the two Fe($NCCH_3$)(NH_3) isomers. See supporting information for comparison of NMR spectra. The ^{15}N–H coupling constants are ~1 Hz larger for the Fe($NCCH_3$)($^{15}NH_3$) isomers in comparison to Fe($^{15}NH_3$)$_2$ present in the sample.

^1H NMR (600 MHz, CD_3CN, 0.25 atm $^{15}NH_3$) δ 2.32 (d, $^1J_{NH}$ = 66.8 Hz, 3H), 0.05 (d, $^1J_{NH}$ = 67.5 Hz, 3H),

$^{15}N\{^1H\}$ NMR (50.6 MHz, CD_3CN, 0.25 atm $^{15}NH_3$) δ -402.1, -433.1

[^{Me}(NCCN)Fe(NH_3)][PF_6]$_2$

An NMR tube fitted with a PTFE valve was charged with [^{Me}(NCCN)Fe($NCCH_3$)$_2$]$^{2+}$ (15.2 mg) and CD_3CN in a nitrogen-filled glovebox. The sample was degassed by three freeze-pump-thaw cycles, then pressurized with $^{15}NH_3$ (1 atm). The sample was shaken to dissolve the $^{15}NH_3$, and the headspace pressure was replenished several times until the pressure change upon opening the sample was minimal. Single crystals suitable for X-ray diffraction were grown by layering a concentrated NMR sample with a pentane buffer layer then layering with Et_2O.

^1H NMR (600 MHz, CD_3CN, 1 atm $^{15}NH_3$) δ 8.76 (s, 1H), 8.18 – 8.14 (m, 2H), 8.12 (d, J = 8.4 Hz, 1H), 7.96 (d, J = 8.4 Hz, 1H), 7.58 – 7.50 (m, 2H), 7.49 (d, J = 1.6 Hz, 1H), 7.27 (d, J = 1.6 Hz, 1H), 6.80 (s, 1H), 4.44 (dt, J = 14.8, 3.6 Hz, 1H), 3.99 (dt, J = 15.4, 3.1 Hz, 1H), 3.67 (dt, J = 14.4, 8.8 Hz, 1H), 2.57 (s, 3H), 2.47 (d, $^1J_{NH}$ = 65.6 Hz, 3H), 2.49 – 2.43 (m, 1H), 2.24 – 2.15 (m, 2H), 1.99 (s, 3H), 0.19 (d, $^1J_{NH}$ = 66.8 Hz, 3H). *Under 0.25 atm $^{15}NH_3$, the Fe–$^{15}NH_3$ signals shift to δ 2.34 and -0.01.*

$^{13}C\{^1H\}$ NMR (151 MHz, CD_3CN, 1 atm $^{15}NH_3$) δ 219.3, 216.0 (d, J_{CN} = 4 Hz), 154.3, 154.2, 154.0, 152.6, 141.6, 139.7, 133.9, 131.3, 128.9, 126.5, 120.9, 118.9, 118.6, 118.4, 111.9, 111.3, 46.9, 46.4, 31.1, 18.2, 17.6.

$^{15}N\{^1H\}$ NMR (60.9 MHz, CD_3CN, 1 atm $^{15}NH_3$) δ -399.2, -430.6

[^{NMe2}(NCCN)Fe($NCCH_3$)$_2$][PF_6]$_2$

In a nitrogen-filled glovebox, ^{NMe2}(NCCN) (116 mg, 0.163 mmol) was dissolved in MeCN (5 mL) and was placed in a -30 °C freezer for 3 h before being added to a suspension of Fe(N($SiMe_3$)$_2$)$_2$ • (THF)$_{0.75}$ (72 mg, 0.169 mmol) in cold MeCN (12 mL, -30 °C). The mixture was stirred for 16 hours at ambient temperature for 18 h before the solvent was reduced in volume under vacuum to ~1.5 mL. The dark red solution was extracted with pentane (3 × 6 mL) to remove hexamethyldisilazane (HN($SiMe_3$)$_2$, HMDS) formed during the reaction. [^{NMe2}(NCCN)Fe($NCCH_3$)$_2$][PF_6]$_2$ was isolated as a dark red crystalline solid by vapor diffusion of Et_2O and pentane (2:1) into a concentrated MeCN solution at ambient temperature. The crystals were crushed and dried under vacuum. Yield: 109 mg, 79%.

^1H NMR (600 MHz, CD_3CN) δ 8.72 (d, J = 6.7 Hz, 1H), 8.16 (d, J = 6.2 Hz, 2H), 7.48 (s, 1H), 7.23 (s, 1H), 7.14 (s, 1H), 6.95 (d, J = 5.0 Hz, 1H), 6.79 (s, 1H), 6.38 (d, J = 6.9 Hz, 1H), 6.21 – 6.12 (m, 1H), 4.49 – 4.37 (m, 2H), 3.99 (d, J = 15.3 Hz, 1H), 3.26 (s, 6H), 3.00 (s, 6H), 2.47 – 2.38 (m, 1H), 2.28 – 2.21 (m, 2H), 1.96 (s, 6H).

$^{13}C\{^1H\}$ NMR (151 MHz, CD_3CN) δ 215.7, 209.2, 158.1, 157.3, 155.9, 155.6, 151.6, 150.6, 128.84 126.1, 120.93, 107.9, 106.2, 94.7, 46.8, 46.6, 40.2 (N(CH_3)$_2$), 39.9 (N(CH_3)$_2$), 31.5.

Anal. Calcd for $C_{27}H_{34}F_{12}FeN_{10}P_2$: C, 38.41; H, 4.06; N, 16.59. Found: C, 37.90; H, 4.09; N, 16.36.

[^{NMe2}(NCCN)Fe(NH_3)($NCCH_3$)][PF_6]$_2$

An NMR tube fitted with a PTFE valve was charged with [^{NMe2}(NCCN)Fe($NCCH_3$)$_2$]$^{2+}$ and CD_3CN in a nitrogen-filled glovebox. The sample was degassed by three freeze-pump-thaw cycles, then pressurized with $^{15}NH_3$ (0.25 atm). The sample was shaken to dissolve the $^{15}NH_3$, and the headspace pressure was replenished several times until the pressure change upon opening the sample was minimal. N_2 was then used to bring the sample to 1 atm total. By ^1H, $^1H\{^{15}N\}$, and $^{15}N\{^1H\}$ NMR spectroscopy, a mixture of $Fe(NH_3)_n(NCCH_3)_m$ species, were observed ($n + m = 2$).

Single crystals suitable for X-ray diffraction studies were obtained at ambient temperature in a glovebox by vapor diffusion of Et_2O into a concentrated MeCN solution of [^{NMe2}(NCCN)Fe(NH_3)$_2$][PF_6]$_2$, where only the MeCN had been sparged with NH_3. NMR data reported below are for signals readily assigned to the two Fe($NCCH_3$)(NH_3) isomers.

^1H NMR (500 MHz, CD_3CN) δ 2.38 (d), -0.17 (d)

$^{15}N\{^1H\}$ NMR (50.7 MHz, CD_3CN) δ -401.5, -433.8

[^{NMe2}(NCCN)Fe(NH_3)$_2$][PF_6]$_2$

An NMR tube fitted with a PTFE valve was charged with [^{NMe2}(NCCN)Fe($NCCH_3$)$_2$]$^{2+}$ and CD_3CN in a nitrogen-filled glovebox. The sample was degassed by three freeze-pump-thaw cycles, then pressurized with $^{15}NH_3$ (1 atm). The sample was shaken to dissolve the $^{15}NH_3$, and the headspace pressure was replenished several times until the pressure change upon opening the sample was minimal. Upon diffusion of NH_3 into solution, the solution turned from red to dark red in color. For NMR characterization, $^{15}NH_3$ was used. Single crystals suitable for X-ray diffraction studies were obtained at ambient temperature in a glovebox by vapor diffusion of Et_2O into a concentrated MeCN solution of [^{NMe2}(NCCN)Fe(NH_3)$_2$][PF_6]$_2$, where both the Et_2O and MeCN had been sparged with NH_3. Resdissolving crystals of [^{NMe2}(NCCN)Fe(NH_3)$_2$]$^{2+}$ in CD_3CN in the absence of additional NH_3 led to a mixture of $Fe(NH_3)_n(NCCH_3)_m$ species ($n + m = 2$).

^1H NMR (600 MHz, CD_3CN, 1 atm $^{15}NH_3$) δ 8.40 (1H), 8.18 (1H), 8.15 (1H), 7.44 (1H), 7.22 (1H), 7.12 (1H), 6.94 (1H), 6.77 (1H), 6.36 (1H), 6.10 (1H), 4.40 (1H), 3.98 (1H), 3.64 (1H), 3.64, 3.25, 3.09, 3.08, 2.98, 2.47, 2.39 (d, $^1J_{NH}$ = 65.7 Hz, 3H)., 2.19, -0.15 (d, $^1J_{NH}$ = 66.6 Hz, 3H).

^{13}C NMR (151 MHz, CD_3CN) δ 222.3, 220.1, 157.8, 156.9, 156.4, 156.0, 151.5, 151.0, 128.6, 126.0, 120.6, 107.4, 105.9, 94.3, 94.1, 46.9, 46.4, 40.2, 39.9, 31.2.

$^{15}N\{^1H\}$ NMR (50.7 MHz, CD_3CN, 1 atm $^{15}NH_3$) δ -398.6 (N1), -431.7 (N2).

^{15}N NMR (60.9 MHz, CD_3CN, 1 atm $^{15}NH_3$) δ -398.6 (q, $^1J_{NH}$ = 65.7 Hz, N1), -431.7 (q, $^1J_{NH}$ = 67.3 Hz, N2)

[(*tetra*-NHC)Fe(NH_3)$_2$][PF_6]$_2$

An NMR tube fitted with a PTFE valve was charged with [[(*tetra*-NHC)Fe($NCCH_3$)$_2$]$^{2+}$ and CD_3CN in a nitrogen-filled glovebox. The sample was degassed by three freeze-pump-thaw cycles, then pressurized with $^{15}NH_3$ (1 atm). The sample was shaken to dissolve the $^{15}NH_3$, and the headspace pressure was replenished several times until the pressure change upon opening the sample was minimal. Upon diffusion of NH_3 into solution, the yellow color of the solution darked slightly to a golden yellow.

^1H NMR (600 MHz, CD_3CN, 1 atm $^{15}NH_3$) δ

$^{15}N\{^1H\}$ NMR (60.9 MHz, CD_3CN, 1 atm $^{15}NH_3$) δ -415.7

ASSOCIATED CONTENT

Supporting Information

NMR spectra and X-ray crystallography methods and structures may be found in the Supporting Information. The Supporting Information is available free of charge on the ACS Publications website. CCDC-2271707-2271711 contains the supplementary crystallographic data for this paper. These data can be obtained free of charge from The Cambridge Crystallographic Data Centre via www.ccdc.cam.ac.uk/data_request/cif.

AUTHOR INFORMATION

Corresponding Author

R. Morris Bullock – Center for Molecular Electrocatalysis, Pacific Northwest National Laboratory, Richland, Washington, 99352, United States; orcid.org/0000-0001-6306-4851; Email: morris.bullock@pnnl.gov

Author Contributions

The manuscript was written through contributions of all authors. All authors have given approval to the final version of the manuscript.

Funding Sources

This work was supported by the Center for Molecular Electrocatalysis, an Energy Frontier Research Center funded by the U.S. Department of Energy, Office of Science, Office of Basic Energy Sciences. No competing financial interests have been declared.

ACKNOWLEDGMENT

ABBREVIATIONS

REFERENCES

(1) (a) Afif, A.; Radenahmad, N.; Cheok, Q.; Shams, S.; Kim, J. H.; Azad, A. K. Ammonia-fed fuel cells: a comprehensive review. *Renew. Sust. Energ. Rev.* **2016**, *60*, 822-835, DOI: https://doi.org/10.1016/j.rser.2016.01.120. (b) Jeerh, G.; Zhang, M.; Tao, S. Recent progress in ammonia fuel cells and their potential applications. *J. Mater. Chem. A* **2021**, *9*, 727-752, DOI: 10.1039/D0TA08810B. (c) Lan, R.; Tao, S. Ammonia as a Suitable Fuel for Fuel Cells. *Front. Energy Res.* **2014**, *2*, . (d) Chehade, G.; Dincer, I. Progress in green ammonia production as potential carbon-free fuel. *Fuel* **2021**, *299*, 120845, DOI: https://doi.org/10.1016/j.fuel.2021.120845. (e) Grinberg Dana, A.; Elishav, O.; Bardow, A.; Shter, G. E.; Grader, G. S. Nitrogen-Based Fuels: A Power-to-Fuel-to-Power Analysis. *Angew. Chem. Int. Ed.* **2016**, *55*, 8798-8805, DOI: https://doi.org/10.1002/anie.201510618.

(2) (a) Collman, J. P.; Hutchison, J. E.; Lopez, M. A.; Guilard, R.; Reed, R. A. Toward a Dinitrogen Electroreduction Catalyst: Characterization of a Bis-Ammine, a μ_2-Hydrazine, a μ_2-Diazene, and a Remarkably Stable μ_2-Dinitrogen Complex of a Ruthenium Cofacial Diporphyrin. *J. Am. Chem. Soc.* **1991**, *113*, 2794-2796, DOI: 10.1021/ja00007a088. (b) Collman, J. P.; Hutchison, J. E.; Ennis, M. S.; Lopez, M. A.; Guilard, R. Reduced nitrogen hydride complexes of a cofacial metallodiporphyrin and their oxidative interconversion. An analysis of ammonia oxidation and prospects for a dinitrogen electroreduction catalyst based on cofacial metallodiporphyrins. *J. Am. Chem. Soc.* **1992**, *114*, 8074-8080, DOI: 10.1021/ja00047a016.

(3) Dunn, P. L.; Johnson, S. I.; Kaminsky, W.; Bullock, R. M. Diversion of Catalytic C–N Bond Formation to Catalytic Oxidation of NH_3 through Modification of the Hydrogen Atom Abstractor. *J. Am. Chem. Soc.* **2020**, *142*, 3361-3365, DOI: 10.1021/jacs.9b13706.

(4) Cook, B. J.; Barona, M.; Johnson, S. I.; Raugei, S.; Bullock, R. M. Weakening the N–H Bonds of NH_3 Ligands: Triple Hydrogen-Atom Abstraction to Form a Chromium(V) Nitride. *Inorg. Chem.* **2022**, *61*, 11165-11172, DOI: 10.1021/acs.inorgchem.2c01115.

(5) Johnson, S. I.; Heins, S. P.; Klug, C. M.; Wiedner, E. S.; Bullock, R. M.; Raugei, S. Design and reactivity of pentapyridyl metal complexes for ammonia oxidation. *Chem. Commun.* **2019**, *55*, 5083-5086, DOI: 10.1039/C9CC01249D.

(6) Cook, B. J.; Johnson, S. I.; Chambers, G. M.; Kaminsky, W.; Bullock, R. M. Triple hydrogen atom abstraction from Mn–NH_3 complexes results in cyclophosphazenium cations. *Chem. Commun.* **2019**, *55*, 14058-14061, DOI: 10.1039/C9CC06915A.

(7) Dunn, P. L.; Barona, M.; Johnson, S. I.; Raugei, S.; Bullock, R. M. Hydrogen Atom Abstraction from an $Os^{II}(NH_3)_2$ Complex Generates an $Os^{IV}(NH_2)_2$ Complex: Experimental and Computational Analysis of the N–H Bond Dissociation Free Energies and Reactivity. *Inorg. Chem.* **2022**, *61*, 15325-15334, DOI: 10.1021/acs.inorgchem.2c00708.

(8) Stephens, D. N.; Szilagyi, R. K.; Roehling, P. N.; Arulsamy, N.; Mock, M. T. Catalytic Ammonia Oxidation to Dinitrogen by a Nickel Complex. *Angew. Chem. Int. Ed.* **2023**, *62*, e202213462, DOI: https://doi.org/10.1002/anie.202213462.

(9) (a) Dunn, P. L.; Cook, B. J.; Johnson, S. I.; Appel, A. M.; Bullock, R. M. Oxidation of Ammonia with Molecular Complexes. *J. Am. Chem. Soc.* **2020**, *142*, 17845-17858, DOI: 10.1021/jacs.0c08269. (b) Galvin, C. M.; Waymouth, R. M. Electron-Rich Phenoxyl Mediators Improve Thermodynamic Performance of Electrocatalytic Alcohol Oxidation with an Iridium Pincer Complex. *J. Am. Chem. Soc.* **2020**, *142*, 19368-19378, DOI: 10.1021/jacs.0c09605.

(10) Toda, H.; Kuroki, K.; Kanega, R.; Kuriyama, S.; Nakajima, K.; Himeda, Y.; Sakata, K.; Nishibayashi, Y. Manganese-Catalyzed Ammonia Oxidation into Dinitrogen under Chemical or Electrochemical Conditions. *ChemPlusChem* **2021**, *86*, 1511-1516, DOI: https://doi.org/10.1002/cplu.202100349.

(11) (a) Zott, M. D.; Garrido-Barros, P.; Peters, J. C. Electrocatalytic Ammonia Oxidation Mediated by a Polypyridyl Iron Catalyst. *ACS Catal.* **2019**, *9*, 10101-10108, DOI: 10.1021/acscatal.9b03499. (b) Zott, M. D.; Peters, J. C. Enhanced Ammonia Oxidation Catalysis by a Low-Spin Iron Complex Featuring *Cis* Coordination Sites. *J. Am. Chem. Soc.* **2021**, *143*, 7612-7616, DOI: 10.1021/jacs.1c02232. (c) Li, Y.; Chen, J.-Y.; Miao, Q.; Yu, X.; Feng, L.; Liao, R.-Z.; Ye, S.; Tung, C.-H.; Wang, W. A Parent Iron Amido Complex in Catalysis of Ammonia Oxidation. *J. Am. Chem. Soc.* **2022**, *144*, 4365-4375, DOI: 10.1021/jacs.1c08609.

(12) (a) Liu, H.-Y.; Lant, H. M. C.; Troiano, J. L.; Hu, G.; Mercado, B. Q.; Crabtree, R. H.; Brudvig, G. W. Electrocatalytic, Homogeneous Ammonia Oxidation in Water to Nitrate and Nitrite with a Copper Complex. *J. Am. Chem. Soc.* **2022**, *144*, 8449-8453, DOI: 10.1021/jacs.2c01788. (b) Ahmed, M. E.; Raghibi Boroujeni, M.; Ghosh, P.; Greene, C.; Kundu, S.; Bertke, J. A.; Warren, T. H. Electrocatalytic Ammonia Oxidation by a Low-Coordinate Copper Complex. *J. Am. Chem. Soc.* **2022**, *144*, 21136-21145, DOI: 10.1021/jacs.2c07977.

(13) (a) Trenerry, M. J.; Wallen, C. M.; Brown, T. R.; Park, S. V.; Berry, J. F. Spontaneous N_2 formation by a diruthenium complex enables electrocatalytic and aerobic oxidation of ammonia. *Nat. Chem.* **2021**, *13*, 1221-1227, DOI: 10.1038/s41557-021-00797-w. (b) Holub, J.; Vereshchuk, N.; Sanchez-Baygual, F. J.; Gil-Sepulcre, M.; Benet-Buchholz, J.; Llobet, A. Synthesis, Structure, and Ammonia Oxidation Catalytic Activity of Ru-NH_3 Complexes Containing Multidentate Polypyridyl Ligands. *Inorg. Chem.* **2021**, *60*, 13929-13940, DOI: 10.1021/acs.inorgchem.1c01528. (c) Jacob, S. I.; Chakraborty, A.; Chamas, A.; Bock, R.; Sepunaru, L.; Ménard, G. Rapid Aqueous Ammonia Oxidation to N_2 Using a Molecular Ru Electrocatalyst. *ACS Energy Lett.* **2023**, *8*, 3760-3766, DOI: 10.1021/acsenergylett.3c01133. (d) Nakajima, K.; Toda, H.; Sakata,

K.; Nishibayashi, Y. Ruthenium-catalysed oxidative conversion of ammonia into dinitrogen. *Nat. Chem.* **2019**, *11*, 702-709, DOI: 10.1038/s41557-019-0293-y. (e) Habibzadeh, F.; Miller, S. L.; Hamann, T. W.; Smith, M. R. Homogeneous electrocatalytic oxidation of ammonia to N_2 under mild conditions. *Proc. Natl. Acad. Sci. U.S.A.* **2019**, *116*, 2849-2853, DOI: 10.1073/pnas.1813368116. (f) Toda, H.; Kuroki, K.; Kanega, R.; Yano, T.; Yoshikawa, T.; Kuriyama, S.; Himeda, Y.; Sakata, K.; Nishibayashi, Y. Catalytic Ammonia Oxidation Using Ammonia Solution under Electrochemical Conditions: Investigation on Axial Ligand of Ruthenium Catalysts. *Bull. Chem. Soc. Jpn.* **2023**, *96*, 980-988, DOI: 10.1246/bcsj.20230136.

(14) Beiler, A. M.; Denisiuk, A.; Holub, J.; Sánchez-Baygual, F.-J.; Gil-Sepulcre, M.; Ertem, M. Z.; Moonshiram, D.; Piccioni, A.; Llobet, A. Heterogeneous Electrochemical Ammonia Oxidation with a Ru-bda Oligomer Anchored on Graphitic Electrodes via CH−π Interactions. *ACS Energy Lett.* **2023**, *8*, 172-178, DOI: 10.1021/acsenergylett.2c02483.

(15) (a) Raba, A.; Cokoja, M.; Ewald, S.; Riener, K.; Herdtweck, E.; Pöthig, A.; Herrmann, W. A.; Kühn, F. E. Synthesis and Characterization of Novel Iron(II) Complexes with Tetradentate Bis(N-heterocyclic carbene)–Bis(pyridine) (NCCN) Ligands. *Organometallics* **2012**, *31*, 2793-2800, DOI: 10.1021/om2010673. (b) Weiss, D. T.; Anneser, M. R.; Haslinger, S.; Pöthig, A.; Cokoja, M.; Basset, J.-M.; Kühn, F. E. NHC Versus Pyridine: How "Teeth" Change the Redox Behavior of Iron(II) Complexes. *Organometallics* **2015**, *34*, 5155-5166, DOI: 10.1021/acs.organomet.5b00732.

(16) (a) Stennett, C. R.; Fettinger, J. C.; Power, P. P. Low-Coordinate Iron Chalcogenolates and Their Complexes with Diethyl Ether and Ammonia. *Inorg. Chem.* **2021**, *60*, 6712-6720, DOI: 10.1021/acs.inorgchem.1c00539. (b) Saouma, C. T.; Lu, C. C.; Peters, J. C. Mononuclear Five- and Six-Coordinate Iron Hydrazido and Hydrazine Species. *Inorg. Chem.* **2012**, *51*, 10043-10054, DOI: 10.1021/ic301704f. (c) Sellmann, D.; Soglowek, W.; Knoch, F.; Ritter, G.; Dengler, J. Transition-metal complexes with sulfur ligands. 88. Dependence of spin state, structure, and reactivity of $[Fe^{II}(L)('NH)S_4')]$ complexes on the coligand L (L = CO, N_2H_2, N_2H_4, NH_3, pyridine, $NHCH_3NH_2$, CH_3OH, THF, $P(OCH_3)_3$, $P(OPh)_3$): model complexes for iron nitrogenases ($'NHS_4'^{2-}$ = dianion of 2,2'-bis[(2-mercaptophenyl)thio]diethylamine). *Inorg. Chem.* **1992**, *31*, 3711-3717, DOI: 10.1021/ic00044a011. (d) Lee, Y.; Mankad, N. P.; Peters, J. C. Triggering N_2 uptake via redox-induced expulsion of coordinated NH_3 and N_2 silylation at trigonal bipyramidal iron. *Nat. Chem.* **2010**, *2*, 558-565, DOI: 10.1038/nchem.660. (e) Chetcuti, P. A.; Liégard, A.; Rihs, G.; Rist, G.; Schweiger, A. Crystal Structure and ESR Study of a Bimetallic Copper/Iron Crown Ether Inclusion Complex. *Helv. Chim. Acta* **1991**, *74*, 1591-1599, DOI: https://doi.org/10.1002/hlca.19910740721. (f) Saouma, C. T.; Moore, C. E.; Rheingold, A. L.; Peters, J. C. A Five-Coordinate Phosphino/Acetate Iron(II) Scaffold That Binds N_2, N_2H_2, N_2H_4, and NH_3 in the Sixth Site. *Inorg. Chem.* **2011**, *50*, 11285-11287, DOI: 10.1021/ic2016066. (g) Chang, Y.-H.; Chan, P.-M.; Tsai, Y.-F.; Lee, G.-H.; Hsu, H.-F. Catalytic Reduction of Hydrazine to Ammonia by a Mononuclear Iron(II) Complex on a Tris(thiolato)phosphine Platform. *Inorg. Chem.* **2014**, *53*, 664-666, DOI: 10.1021/ic402108w. (h) McQuarters, A. B.; Goodrich, L. E.; Goodrich, C. M.; Lehnert, N. Disproportionation of O-Benzylhydroxylamine Catalyzed by a Ferric Bis-Picket Fence Porphyrin Complex. *Z. Anorg. Allg. Chem.* **2013**, *639*, 1520-1526, DOI: https://doi.org/10.1002/zaac.201300125. (i) Heiden, Z. M.; Chen, S.; Mock, M. T.; Dougherty, W. G.; Kassel, W. S.; Rousseau, R.; Bullock, R. M. Protonation of Ferrous Dinitrogen Complexes Containing a Diphosphine Ligand with a Pendent Amine. *Inorg. Chem.* **2013**, *52*, 4026-4039, DOI: 10.1021/ic4000704. (j) Sickerman, N. S.; Peterson, S. M.; Ziller, J. W.; Borovik, A. S. Synthesis, structure and reactivity of $Fe^{II/III}$–NH_3 complexes bearing a tripodal sulfonamido ligand. *Chem. Commun.* **2014**, *50*, 2515-2517, DOI: 10.1039/C3CC48804G. (k) Anderson, J. S.; Moret, M.-E.; Peters, J. C. Conversion of Fe–NH_2 to Fe–N_2 with release of NH_3. *J. Am. Chem. Soc.* **2013**, *135*, 534-537, DOI: 10.1021/ja307714m. (l) Creutz, S. E.; Peters, J. C. Exploring secondary-sphere interactions in Fe–N_xH_y complexes relevant to N_2 fixation. *Chem. Sci.* **2017**, *8*, 2321-2328, DOI: 10.1039/C6SC04805F. (m) Bowman, A. C.; Bart, S. C.; Heinemann, F. W.; Meyer, K.; Chirik, P. J. Synthesis of Bis(imino)pyridine Iron Amide and Ammonia Compounds from an N−H Transfer Agent. *Inorg. Chem.* **2009**, *48*, 5587-5589, DOI: 10.1021/ic9003017. (n) Vela, J.; Stoian, S.; Flaschenriem, C. J.; Münck, E.; Holland, P. L. A Sulfido-Bridged Diiron(II) Compound and Its Reactions with Nitrogenase-Relevant Substrates. *J. Am. Chem. Soc.* **2004**, *126*, 4522-4523, DOI: 10.1021/ja049417l. (o) Nurdin, L.; Yang, Y.; Neate, P. G. N.; Piers, W. E.; Maron, L.; Neidig, M. L.; Lin, J.-B.; Gelfand, B. S. Activation of ammonia and hydrazine by electron rich Fe(II) complexes supported by a dianionic pentadentate ligand platform through a common terminal Fe(III) amido intermediate. *Chem. Sci.* **2021**, *12*, 2231-2241, DOI: 10.1039/D0SC06466A. (p) Sun, C.; Oswald, V. F.; Hill, E. A.; Ziller, J. W.; Borovik, A. S. Investigation of iron–ammine and amido complexes within a C_3-symmetrical phosphinic amido tripodal ligand. *Dalton Trans.* **2021**, *50*, 11197-11205, DOI: 10.1039/D1DT01032H. (q) Fox, D. J.; Bergman, R. G. Synthesis of an Iron Parent Amido Complex and a Comparison of Its Reactivity with the Ruthenium Analog. *Organometallics* **2004**, *23*, 1656-1670, DOI: 10.1021/om0499660. (r) Wang, Z.; Johnson, S. I.; Wu, G.; Ménard, G. Multiple N–H and C–H Hydrogen Atom Abstractions Through Coordination-Induced Bond Weakening at Fe-Amine Complexes. *Inorg. Chem.* **2021**, *60*, 8242-8251, DOI: 10.1021/acs.inorgchem.1c00923.

(17) Little, D. J.; Edwards, D. O.; Smith, M. R.; Hamann, T. W. As Precious as Platinum: Iron Nitride for Electrocatalytic Oxidation of Liquid Ammonia. *ACS Appl. Mater. Interfaces* **2017**, *9*, 16228-16235, DOI: 10.1021/acsami.7b02639.

(18) Watt, G. W.; Chrisp, J. D. Spectrophotometric Method for Determination of Hydrazine. *Anal. Chem.* **1952**, *24*, 2006-2008, DOI: 10.1021/ac60072a044.

(19) Weiss, D. T.; Altmann, P. J.; Haslinger, S.; Jandl, C.; Pöthig, A.; Cokoja, M.; Kühn, F. E. Structural diversity of late transition metal complexes with flexible tetra-NHC ligands. *Dalton Trans.* **2015**, *44*, 18329-18339, DOI: 10.1039/C5DT02386F.

(20) Nazeeruddin, M. K.; Zakeeruddin, S. M.; Kalyanasundaram, K. Enhanced intensities of the ligand-to-metal charge-transfer transitions in ruthenium(III) and osmium(III) complexes of substituted bipyridines. *J. Phys. Chem.* **1993**, *97*, 9607-9612, DOI: 10.1021/j100140a014.

(21) Coetzee, J. F.; Padmanabhan, G. R. Properties of Bases in Acetonitrile as Solvent. IV. Proton Acceptor Power and Homoconjugation of Mono- and Diamines. *J. Am. Chem. Soc.* **1965**, *87*, 5005-5010, DOI: 10.1021/ja00950a006.

(22) Tshepelevitsh, S.; Kütt, A.; Lõkov, M.; Kaljurand, I.; Saame, J.; Heering, A.; Plieger, P. G.; Vianello, R.; Leito, I. On the Basicity of Organic Bases in Different Media. *Eur. J. Org. Chem.* **2019**, *2019*, 6735-6748, DOI: https://doi.org/10.1002/ejoc.201900956.

(23) TMG addition to $[^{NMe2}(NCCN)Fe(NCCH_3)_2]^{2+}$ does not support simple binding of TMG to the Fe(III). See Supporting Information.

(24) Fulmer, G. R.; Miller, A. J. M.; Sherden, N. H.; Gottlieb, H. E.; Nudelman, A.; Stoltz, B. M.; Bercaw, J. E.; Goldberg, K. I. NMR Chemical Shifts of Trace Impurities: Common Laboratory Solvents, Organics, and Gases in Deuterated Solvents Relevant to the Organometallic Chemist. *Organometallics* **2010**, *29*, 2176-2179, DOI: 10.1021/om100106e.

(25) Raba, A.; Anneser, M. R.; Jantke, D.; Cokoja, M.; Herrmann, W. A.; Kühn, F. E. Facile and scalable preparation of 2-imidazolylpyridines. *Tetrahedron Lett.* **2013**, *54*, 3384-3387, DOI: https://doi.org/10.1016/j.tetlet.2013.04.060.

(26) Manner, V. W.; Markle, T. F.; Freudenthal, J. H.; Roth, J. P.; Mayer, J. M. The first crystal structure of a monomeric phenoxyl radical: 2,4,6-tri-tert-butylphenoxyl radical. *Chem. Commun.* **2008**, 256-258, DOI: 10.1039/B712872J.

(27) Peters, M.; Breinbauer, R. A simple synthesis of functionalized 3-methyl-1-pyridinyl-1H-imidazolium salts as bidentate N-heterocyclic-carbene precursors and their application in Ir-catalyzed arene borylation. *Tetrahedron Lett.* **2010**, *51*, 6622-6625, DOI: https://doi.org/10.1016/j.tetlet.2010.10.059.

Insert Table of Contents artwork here